Research Article
P-ISSN: 2971-785X, E-ISSN: 3141-4095
NIGERIAN JOURNAL OF ENGINEERING RESEARCH UNICROSS (NJERU)
DOI: 10.67571/njeru.2026.010919
Volume 3, Issue 1, 25 march 2026, 9-19

Coordination Control of Battery Energy Storage System and Supercapacitors for High-Frequency PV Smoothing in Microgrids

Peter O. Ohiero [a*]

[a] Department of Electrical and Electronic Engineering, Faculty of Engineering, University of Cross River State, Calabar, Nigeria.

[*]Corresponding author: peterohiero@unicross.edu.ng

Received:8 December 2025 Revised:10 February 2026 Accepted: 27 February 2026

ABSTRACT

The high penetration of Photovoltaic (PV) systems in modern microgrids introduces significant power quality challenges, specifically high-frequency power fluctuations caused by intermittent irradiance and cloud transients. While Battery Energy Storage Systems (BESS) are widely used for energy management, their low power density and limited cycle life make them inadequate for mitigating high-frequency transients. This paper proposes a novel coordinated control strategy for a Hybrid Energy Storage System (HESS) integrating BESS and Supercapacitors (SCs). The proposed configuration employs an Adaptive Frequency-Splitting (AFS) algorithm based on a variable coefficient Low-Pass Filter (LPF). Simulation results demonstrate that the proposed coordination control reduces the battery's peak current stress by 42.5% and stabilizes the DC bus voltage within a 1.2% deviation range, potentially extending battery cycle life by approximately 29%.

Keywords— *Adaptive Frequency Splitting, Battery energy storage system, High-Frequency Smoothing, Hybrid Energy Storage System (HESS), Microgrid Control, Supercapacitors.*

I. INTRODUCTION

The global transition toward sustainable energy systems and climate change mitigation has led to a rapid increase in the installation of Photovoltaic (PV) power plants within microgrid frameworks [1][2]. However, the inherent volatility of solar irradiance, characterized by rapid cloud-edge effects, introduces high-frequency power fluctuations that compromise grid frequency regulation and voltage stability [3]. In autonomous microgrids, these transients can lead to severe power quality degradation and, in extreme cases, unintended load shedding [4].

To mitigate these effects, Energy Storage Systems (ESS) are conventionally deployed to smooth the PV output. Among various technologies, the Battery Energy Storage System (BESS) is the most common due to its high energy density and established commercial maturity [5], [6]. However, BESS faces significant technical hurdles when tasked with high-frequency smoothing. Frequent, high-magnitude power bursts accelerate electrochemical degradation, leading to micro cycling and thermal runaway risks.

Recent research confirms that subjecting Lithium-ion batteries to high-frequency transients, such as current ripples from power electronics or rapid grid frequency regulation, can significantly accelerate degradation compared to conventional cycling [7], [8].

To address the limitations of standalone BESS, the Hybrid Energy Storage System (HESS) has emerged as a superior alternative. By combining BESS with Supercapacitors (SCs), which possess high power density and nearly infinite cycle life, the system can decouple energy and power requirements [9]. In this configuration, the SC handles the rapid, high-frequency transients, while the BESS manages the slower, bulk energy shifts reducing the degradation of the battery by 52% and can extend the operational life of utility-scale BESS by over 30% [9], [10]. The integration of Hybrid Energy Storage Systems (HESS) for smoothing renewable energy fluctuations has been a subject of intense research over the last decade. Emphasis is broadly laid on system sizing, frequency-domain power allocation, and advanced control topologies.

The fundamental rationale for HESS lies in the contrasting physical properties of the storage mediums. Batteries, typically Lead-Acid or Lithium-Ion, offer high energy density (approx. 100 – 200 Wh/kg) but suffer from limited cycle life (2,000 - 5,000 cycles) and slow power response [11]. Conversely, Supercapacitors (SCs) exhibit high power density (up to 10 kW/kg) and exceptional cycle life (>500,000 cycles), albeit with low energy density [12]. Diverting high-frequency transients to SCs can reduce the Root-Mean-Square (RMS) current stress on the battery, thereby significantly mitigating the internal heating and chemical degradation.

The core challenge in HESS coordination is the splitting of the power reference. Current literature explores various coordination strategies for HESS, such as traditional Low-Pass Filters (LPF) [13],

Discrete Wavelet Transform (DWT) [14], and Model Predictive Control (MPC) [15]. While WT offers excellent frequency localization decomposition of signals into multiple frequency bands, providing precise allocation for BESS and SC, its high computational complexity and the inherent sliding window delay in DWT makes real-time implementation challenging in low-cost microgrid controllers. Conversely, while fixed frequency LPFs are simple to implement, they lack adaptability to the State-of-Charge (SoC) of the SC, often leading to saturation or deep discharge during prolonged periods of irradiance cloud cover volatility [13]. MPC-based strategies, as discussed in [15], utilize a receding horizon to optimize power distribution while considering converter constraints and battery health models. While effective, the high computational burden of MPC requires powerful Digital Signal Processors (DSPs), which may not be feasible for distributed small-scale microgrids

Recent advancements in intelligent control have introduced Fuzzy Logic and Machine Learning to optimize HESS power allocation [16], [17], [18]. Furthermore, artificial intelligence techniques, such as Reinforcement Learning (RL), are being explored to predict PV fluctuations and pre-charge SCs, though these are still in the early stages of field validation [19], [20].

Despite the advancements in HESS control, most existing studies focus either on long-term energy management or short-term frequency support in isolation. There is a lack of integrated coordination strategies that simultaneously address high-frequency PV smoothing while maintaining the DC-link voltage stability and ensuring battery longevity through adaptive frequency splitting. This paper proposes an Adaptive Frequency-Splitting (AFS) coordination strategy designed to allocate high-frequency transients to SCs and low-frequency trends to the BESS, thereby optimizing asset longevity and grid stability.

The primary contributions of this research include:

i. The development of an Adaptive Frequency splitting (AFS) control whose time constant τ_{adj} is adjusted based on the SC State-of-Charge (SoC_{sc}) and the rate of change of PV power.

ii. A comprehensive mathematical model of the HESS interface that minimizes DC bus voltage ripples during extreme transients.

iii. A comparative performance evaluation showing the reduction in battery capacity fade through frequency-domain power allocation.

The remainder of this paper is organized as follows: Section 2 describes the microgrid system configuration; Section 3 details the proposed coordination control strategy; Section 4 presents the simulation results and discussion; and Section 5 concludes the work.

II. SYSTEM CONFIGURATION

Figure 1 shows the configuration of the three-phase grid connected solar PV system with BESS and Supercapacitor. The system consists of several power electronic stages that work together to manage energy flow between the solar PV, a DC source, BESS, supercapacitor and the AC grid. It consists of Solar PV Array, Battery (BESS), Supercapacitor (SC), the DC-Link and Conversion, a three-Phase Inverter and filters. The solar PV array is the primary power generator. It uses a DC - DC Boost converter with Maximum Power Point Tracking (MPPT) to ensure it generates the most power possible based on the sun's intensity. The Battery Energy Storage System (BESS) handles the bulk energy storage, providing power during the night or cloudy periods while the Supercapacitor (SC) handles high-frequency power fluctuations, such as sudden motor starts or rapid changes in solar irradiance, protecting the battery from stress. All these sources meet at a common DC-Link

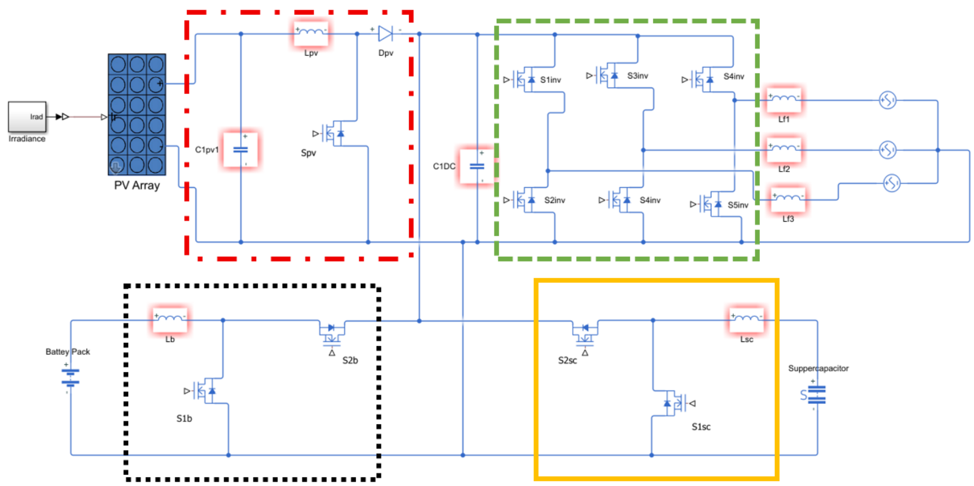

PV DC-DC Boost Converter, Three Phase Inverter, Battery bidirectional DC – DC Converter, Supercapacitor bidirectional DC – DC Converter

FIGURE 1: CONFIGURATION OF THE PV/BESS/SC MICROGRID

The solar PV array is connected to the DC link through a DC – DC boost converter. The Battery and Supercapacitor are connected to the common DC-bus via bi-directional DC - DC converters. This allows them to both charge (absorb excess solar) and discharge (supply the load/grid). The DC link is connected to the AC grid via a three-phase inverter which then converts this DC voltage into AC power to synchronize with the utility grid through a LCL-type AC grid-link filter. Since the system is grid-connected, the inverter is responsible for the DC-bus voltage control. Hence, to maintain a stable DC-bus voltage at the reference value of 700 V, a voltage controller is used, where a reference magnitude for the grid current, and hence the inverter output current, is obtained.

A. Photovoltaic System Model

The PV array is modelled using the standard single-diode equivalent circuit [21]. The output current I_{pv} is expressed as:

$$I_{pv} = I_{ph} - I_0\left[\exp\left(\frac{V_{pv}+I_{pv}R_s}{nKT/q}\right) - 1\right] - \frac{V_{pv}+I_{pv}R_s}{R_{sh}} \quad (1)$$

Where I_{ph} is the photocurrent, and R_s, R_{sh} represent the series and shunt resistances, respectively.

B. Battery and Supercapacitor Dynamics

The BESS is modelled using a modified shepherd model to capture the voltage-current relationship during transient states as presented in [22], [23]. It builds upon the original Shepherd equation by adding an exponential voltage term, a polarization voltage and resistance to better reflect the non-linear behavior of modern batteries such as Li-ion and Lithium Iron Phosphate (LFP or LiFePO4) across their full discharge cycle. The terminal voltage of the battery during charging and discharging are given by;

$$V_{bat_{ch}}(t) = E_0 - K\frac{Q}{it - 0.1Q}\big(it + i(t)\big) + Ae^{-Bit} - R_o(t) \quad (2)$$

$$V_{bat_{dis}}(t) = E_0 - K\frac{Q}{Q - it}(it + i(t)) + Ae^{-Bit} - R_o(t) \quad (3)$$

Where, $V_{bat_{ch}}$ *and* $V_{bat_{dis}}$ are the terminal voltage of the battery in volts (V) at instant t during charging and discharging of the battery respectively, E_0 is the constant battery voltage (V), K is the polarization constant (V/Ah) or polarization resistance (Ω), Q is the maximum battery capacity (Ah), $it = \int i\,dt$ is the extracted capacity (Ah), A is exponential zone amplitude (V), B is e exponential zone time constant inverse (Ah^{-1}), $i(t)$ is low-frequency current dynamics (filtered current) in instant t and R_o is the battery internal resistance, in Ω. The constants A, B, K are obtained from the manufacturer manual. The State-of-Charge (SoC_{bat}) is updated via Coulomb counting:

$$SoC_{bat}(t) = SoC_{bat}(0) - \frac{1}{C_{bat}}\int_0^t i_{bat}\,(k)dk \quad (4)$$

The SC is modelled as an ideal capacitor in series with an Equivalent Series Resistance (ESR), which is critical for calculating heat losses during high-frequency cycles [24]. The terminal voltage of the supercapacitor (V_{sc}) is the sum of the voltage across the ideal capacitor (V_c) and the voltage drop across the ESR (R_{esr}) given as;

$$V_{sc} = V_c - i_{sc}R_{esr} \quad (5)$$

Where the internal capacitor voltage is given by;

$$V_c = \frac{1}{C_{sc}}\int i_{sc}dt + V_c(0) \quad (6)$$

While, the energy stored in the SC is given by $E_{sc} = \frac{1}{2}C_{sc}{V_{sc}}^2$, and its SoC is managed to stay within a high efficiency window of 50% - 100% of its rated voltage.

C. Transfer functions for the Bi-directional DC - DC converters

To control a bi-directional DC - DC converter (typically a Boost-Buck topology), we use transfer functions to understand how a change in the Duty Cycle (d) affects the Output Voltage (Vo) or Inductor Current (i_L). Since the converter operates in two modes (Buck for charging, and Boost for discharging), the transfer functions change depending on the direction of power flow and the assumption that the converter is operating in Continuous Conduction Mode (CCM) and the focus on the Small-Signal Model.

Boost Mode (Discharging to DC-Link)

When the battery or SC is providing power to the DC bus during low or absence of solar, the converter acts as a Boost. The most critical transfer function for control is the Duty-to-Output Voltage $G_{vd}(s)$ given as [25]:

$$G_{vd}(s) = \frac{\hat{v}_o(s)}{\hat{d}(s)} = \frac{V_{in}}{(1-D)^2}\cdot\frac{(1 - s\frac{L}{R(1-D)^2})}{1 + s\frac{L}{R(1-D)^2} + s^2\frac{LC}{(1-D)^2}} \quad (7)$$

The term $1 - s\frac{L}{R(1-D)^2}$ in the numerator is a Right-Half Plane Zero (RHPZ). It means if you suddenly increase the duty cycle to get more voltage, the voltage actually drops momentarily before rising. This makes Boost converters trickier to stabilize than Buck converters.

Buck Mode (Charging from DC-Link)

When excess solar is charging the storage, the converter acts as a Buck. The transfer function is much more stable given by;

$$G_{vd}(s) = \frac{\hat{v}_o(s)}{\hat{d}(s)} = V_{in}\cdot\frac{1}{1 + s\frac{L}{R} + s^2LC} \quad (8)$$

Inner Current Loop Transfer Function

In HESS control, we usually don't control voltage directly; we control the Inductor Current (i_L) first because it's faster. The Duty-to-Inductor Current transfer function $G_{id}(s)$ for a Boost converter is:

$$G_{id}(s) = \frac{\hat{\imath}_L(s)}{\hat{d}(s)} = \frac{2V_o}{R(1-D)^2}\cdot\frac{1 + s\frac{RC}{2}}{1 + s\frac{L}{R(1-D)^2} + s^2\frac{LC}{(1-D)^2}} \quad (9)$$

Applying the Transfer Function to HESS

In this system with a Battery and a Supercapacitor, the Time Constants (T) in these transfer functions are what differentiate the two: For the Battery, the controller is designed to be slow. The bandwidth (f_c)

of the closed - loop transfer function is intentionally limited to ensure the battery doesn't respond to high-frequency noise. While, for the Supercapacitor the controller is designed to be fast. The SC converter's transfer function is tuned with high gain at high frequencies to catch the transients that the battery's slow loop misses.

D. Closed-Loop Control Logic

To make the physical converter follow the Frequency Splitting commands, the transfer functions are wrapped in a PI Controller:

$$C(s) = K_p + \frac{K_i}{s} \tag{10}$$

The loop gain given by the equation below must be designed to have a phase margin of 45^0 to 60^0 to prevent the system from oscillating.

$$T(s) = C(s) \,.\, G_{id}(s) \,.\, H(s) \tag{11}$$

Where H is the sensor gain.

To ensure the supercapacitor (SC) reacts faster than the battery, the bandwidth separation method is used. The SC current control loop is designed to have a much higher Cross Frequency (f_c) than the battery loop. For supercapacitor, the loop bandwidth is between 100Hz - 500Hz, fast and transient while the loop bandwidth for battery is between 1Hz - 10Hz slow and steady. At high frequencies, the inductor impedance dominates, therefore simplifying the model to a first-order system, the duty-current transfer ratio is;

$$G_{id}(s) = \frac{V_{dc}}{sL_{sc}} \tag{12}$$

Where V_{dc} is the DC-link voltage and L_{sc} is the SC interface inductor.

In practical applications, the speed of the system is determined by the proportional gain. For the loop gain $T(s)$ to cross 0 dB at the desired cross over frequency ω_c (where ($\omega_c = 2\pi f_c$).

$$|C(s).G_{id}(s)| \approx 1 \tag{13}$$

DC Bus Voltage and AC inverter side control

$$K_p \,.\, \frac{V_{dc}}{\omega_c L_{sc}} = 1 \tag{14}$$

Making K_p the subject,

$$K_p = \frac{\omega_c L_{sc}}{V_{dc}} \tag{15}$$

The integral gain of the PI controller eliminates steady-state error. To ensure stability and good phase margin, the zero of the PI controllers is set to be 10 times lower than the crossover frequency given as;

$$\frac{K_i}{K_p} = \frac{\omega_c}{10} \tag{16}$$

Rearranging for K_i:

$$K_i = K_p \,.\, \frac{\omega_c}{10} \tag{17}$$

This makes K_i to be higher that K_p at a desired crossover frequency. When (15) and (17) are applied to battery with a lower cross over frequency, the proportional gain K_p is smaller compared to that of supercapacitor which makes the battery ignore rapid changes in the DC-link voltage while the SC responds instantly and faster to the slightest ripple or spikes in the DC-link voltage.

III. Proposed Coordination Control Strategy

The proposed methodology focuses on an integrated control framework that manages the power flow between the PV array, BESS, and SC. The objective is to ensure that high-frequency transients are suppressed by the SC, while the BESS maintains the energy balance of the microgrid.

A. System Energy Balance Modeling

The microgrid architecture utilizes a common DC bus configuration. The instantaneous power balance equation at the DC link is expressed as:

from $$P_{pv}(t) + P_{BESS}(t) + P_{sc}(t) = P_{load}(t) + P_{grid}(t) + P_{loss}(t) \tag{18}$$

Where P_{pv} is the PV generated power, P_{BESS} and P_{sc} are the battery and supercapacitor powers (positive for discharge), P_{grid} is the power exchange with the utility grid and P_{loss} is the power losses [26]. To smooth the PV output, the targeted power to be injected into the grid (P_{smooth}) is derived by passing P_{pv} through a primary smoothing filter;

$$P_{smooth}(s) = \frac{1}{Ts+1} P_{pv}(s) \tag{19}$$

Hence, the total power required from the HESS (P_{hess}) is this:

$$P_{hess} = P_{smooth} - P_{pv} \tag{20}$$

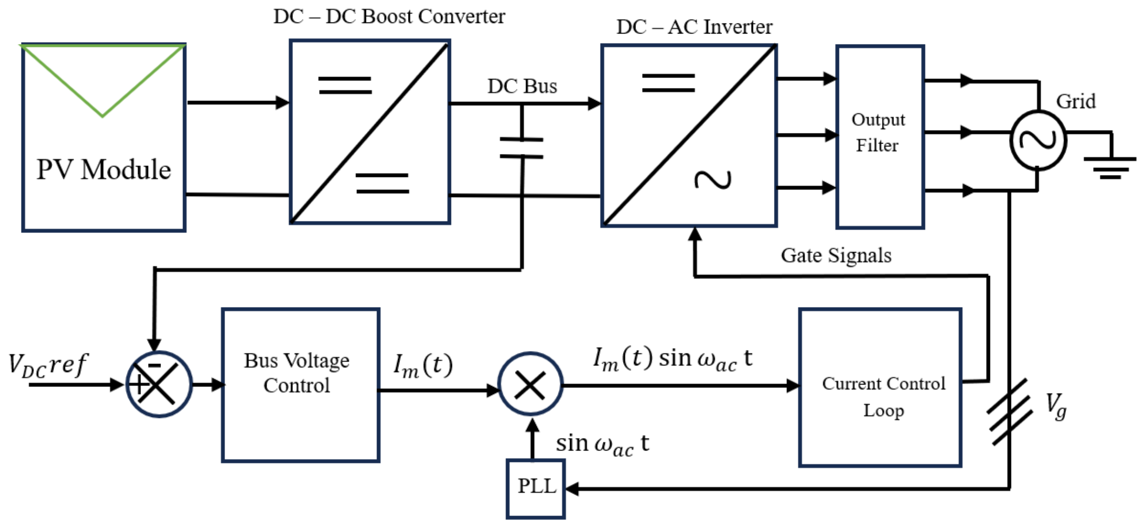

FIGURE 2: A THREE-PHASE GRID CONNECTED PV SYSTEM WITH DC BUS VOLTAGE AND AC SIDE INVERTER CONTROL

B. Adaptive Frequency-Splitting (AFS) Control

To allocate P_{hess} between the BESS and SC, a secondary frequency-splitting layer is implemented. Traditional methods use a fixed time constant, which often leads to SC saturation. In this study, we propose an Adaptive Low-Pass Filter (ALPF). The battery power reference ($P_{BESS}ref$) is obtained as:

$$P_{BESS}ref(s) = \frac{1}{\tau_{adj}s+1} P_{hess}(s) \qquad (21)$$

The remaining high-frequency component is assigned to the SC;

$$P_{sc}ref = P_{hess} - P_{BESS}ref \qquad (22)$$

The innovation lies in the dynamic adjustment of the time constant τ_{adj} based on the SC State-of-Charge (SoC_{sc}).

$$\tau_{adj} = \tau_{nom}.f(SoC_{sc,}\Delta P_{pv}) \qquad (23)$$

Where τ_{nom} is the nominal time constant and f is the non-linear weighting function designed to increase τ when the SC is nearing its energy limits, effectively shifting more load to the battery to protect the SC from depletion.

C. Converter Control and DC Bus Stability

The BESS and SC are interfaced via bidirectional boost-buck converters as shown in Figure 1. A cascaded control loop is employed: an outer voltage loop maintains the DC bus at the reference value ($V_{DC}ref$), and the inner current loops track the battery reference I_bref and supercapacitor $I_{sc}ref$.

To improve the transient response, a feed forward compensation term based on the PV power derivative ($\frac{dP_{pv}}{dt}$) is integrated into the SC current loop, allowing the SC to react to irradiance changes before they manifest as significant DC bus voltage deviations.

D. DC - DC Converter Pulse Width Modulation (PWM)

The physical implementation of the control laws occurs at the bidirectional DC - DC converters. We utilize a Space Vector PWM (SVPWM) to drive the IGBT switches. The inner current control loop is implemented using a Proportional-Integral (PI) regulator tuned via the Ziegler-Nichols method to ensure a phase margin of at least 60^0 for system stability. The feed-forward compensation for PV power fluctuations is implemented by adding the term D_{ff} to the duty cycle:

$$D_{ff} = \frac{V_{dc}-V_{source}}{V_{dc}} \qquad (24)$$

This allows the HESS to anticipate DC bus voltage drops caused by sudden cloud cover

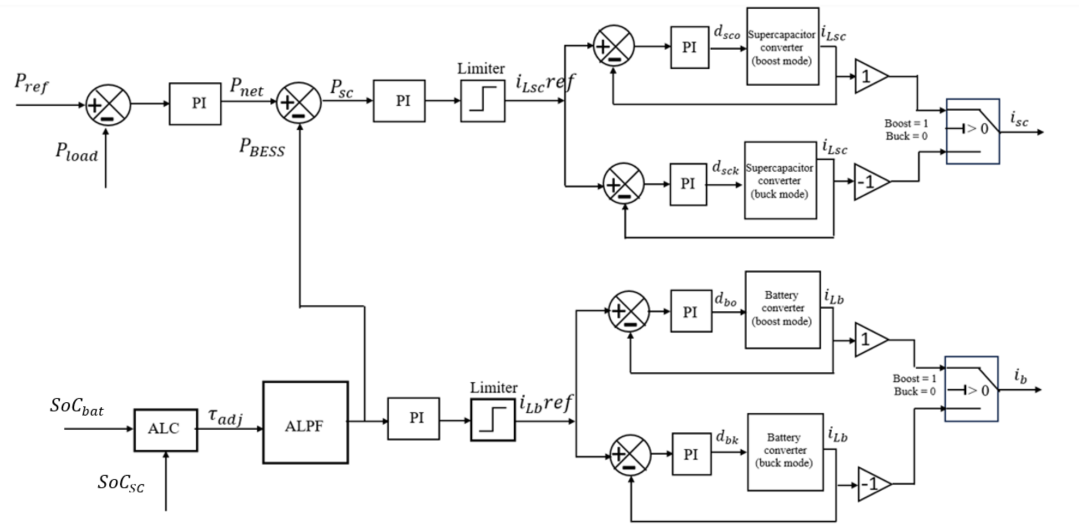

FIGURE 3: BLOCK DIAGRAM OF SUPERCAPACITOR AND BATTERY CURRENT CONTROL

IV. SIMULATION RESULTS AND DISCUSSIONS

To evaluate the efficacy of the proposed adaptive frequency splitting coordination strategy, a high-fidelity numerical model of the microgrid was developed and implemented in MATLAB/Simulink. The PV plant is modeled using real-world solar irradiance data with a resolution obtained from the National Renewable Energy Laboratory (NREL) and Nigerian Meteorological Agency (NiMET) database [27], [28]. The simulation environment accounts for the non-linear dynamics of the power electronic interfaces and the electrochemical characteristics of the storage units.

The first step in implementation involves the real-time acquisition of PV power (P_pv) and load demand (P_load). To isolate high-frequency components, the raw data is sampled at a frequency of 10kHz to capture sub-second transients accurately. Table 1 shows the system parameters used in the simulation. The DC bus nominal voltage is set at 700V, and the PV array is rated at 500kW peak.

A sudden irradiance step change from 800A/m^2 to 200W/m^2 was implemented at 20s to demonstrate a cloud passing scenario and to test the SC's instantaneous response.

Figure 4 compares PV Power, the BESS power output, the SC power output and the net grid power when cloud passing scenario occurs.

TABLE I

SYSTEM PARAMETERS FOR SIMULATION

Parameter	Symbol	Value
PV Nominal Power	P_{pv}	500kW
BESS Capacity	C_{bat}	12V, 7,500Ah
SC Capacitance	C_{sc}	165F, ESR < 1mΩ
DC Bus voltage	V_{dc}	700V
Switching Frequency	f_{sw}	10kHz

Note that positive (+) values indicate discharging into the grid; negative (-) values indicate charging (storing energy).

The performance of the proposed adaptive coordination control was evaluated against a baseline standalone BESS and a conventional fixed-frequency HESS splitting strategy The analysis focuses on three key metrics: PV power smoothing effectiveness, DC bus voltage regulation, and battery current stress reduction. When the sky was clear, the solar PV system generated 450kW into the grid. This happens from 0s to 20s. At this time, BESS and SC did not generate any power into the grid. At 20s and 40s, when the PV drops and rises most violently, the SC absorbs the largest chunk of power to prevent grid voltage flicker.

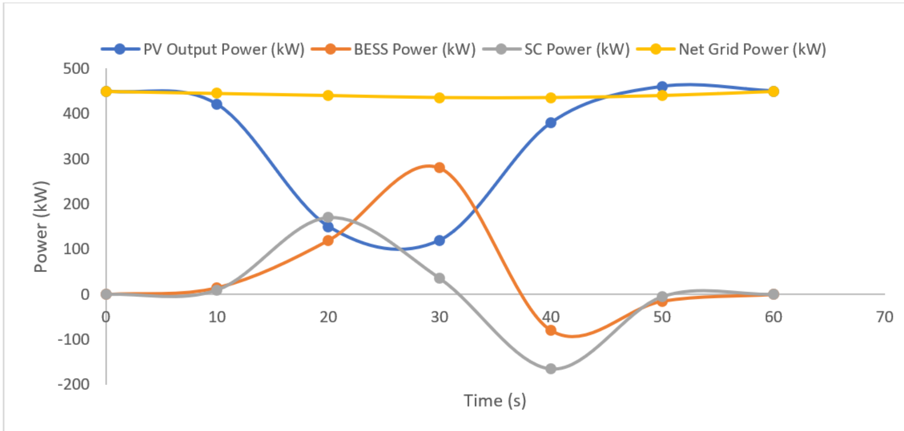

FIGURE 4: RMS OF PV POWER OUTPUT WITH CLOUD PASSING, BESS POWER, SUPERCAPACITOR POWER AND AC GRID POWER

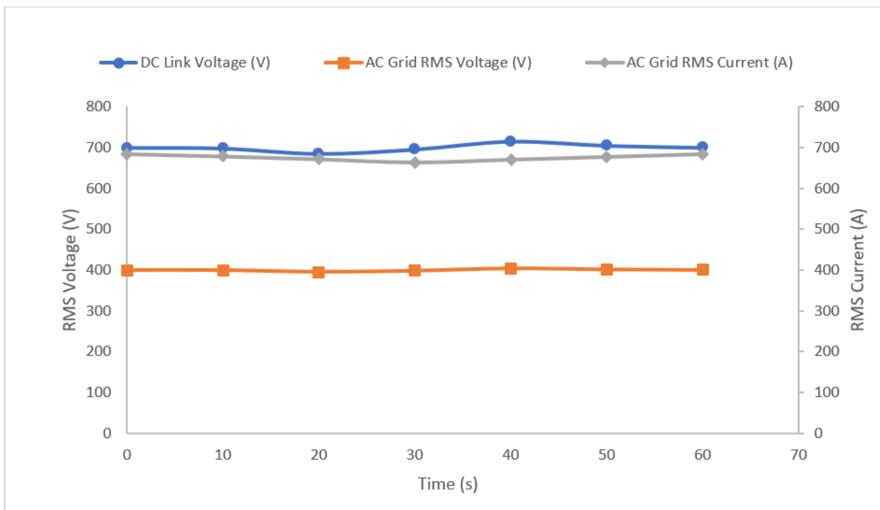

FIGURE 5: THE RMS OF DC LINK VOLTAGE, AC GRID VOLTAGE AND GRID CURRENT

At 30s, once the initial shock of the cloud is over, the BESS provides the sustained energy needed to maintain the grid target while the SC resets its state of charge. This prevents the BESS from having to react to the initial millisecond-scale spike, which significantly extends the battery's cycle life. Notice that while the PV Output swings wildly from 450 kW down to 120 kW (a 73% drop), the Grid Power only changes by ~2% (from 450 kW to 435 kW). Figure 6 show the waveforms of the AC grid voltage and current. Together, BESS and SC maintain the DC Bus voltage which is the critical bridge between solar panels and the grid ensuring the inverter produces clean AC waveforms. When the control system is functioning correctly, the high-frequency noise from the PV system is filtered out before it reaches the grid. Even at 20s (75% power drop), the three-phase AC signals remain purely sinusoidal because the DC Bus is stabilized by the Supercapacitor. At t = 40s (sudden sun return), the PV current spikes. The Supercapacitor absorbs 245 kW in milliseconds suppressed the transient. This prevents the DC Bus voltage from overshooting thereby staying at 712.8V instead of spiking to 900V+, which keeps the AC inverter from clipping or distorting the sinusoidal current. By handling high-frequency fluctuations, the SC filtering the harmonic reduces the Total Harmonic Distortion (THD).

Without the SC, the grid current would show jagged steps as the BESS is slower and struggles to track the cloud edges. The BESS ensures the RMS AC voltage doesn't drift outside of standard utility limits, thereby maintaining a stiff grid connection despite the intermittent solar fuel source.

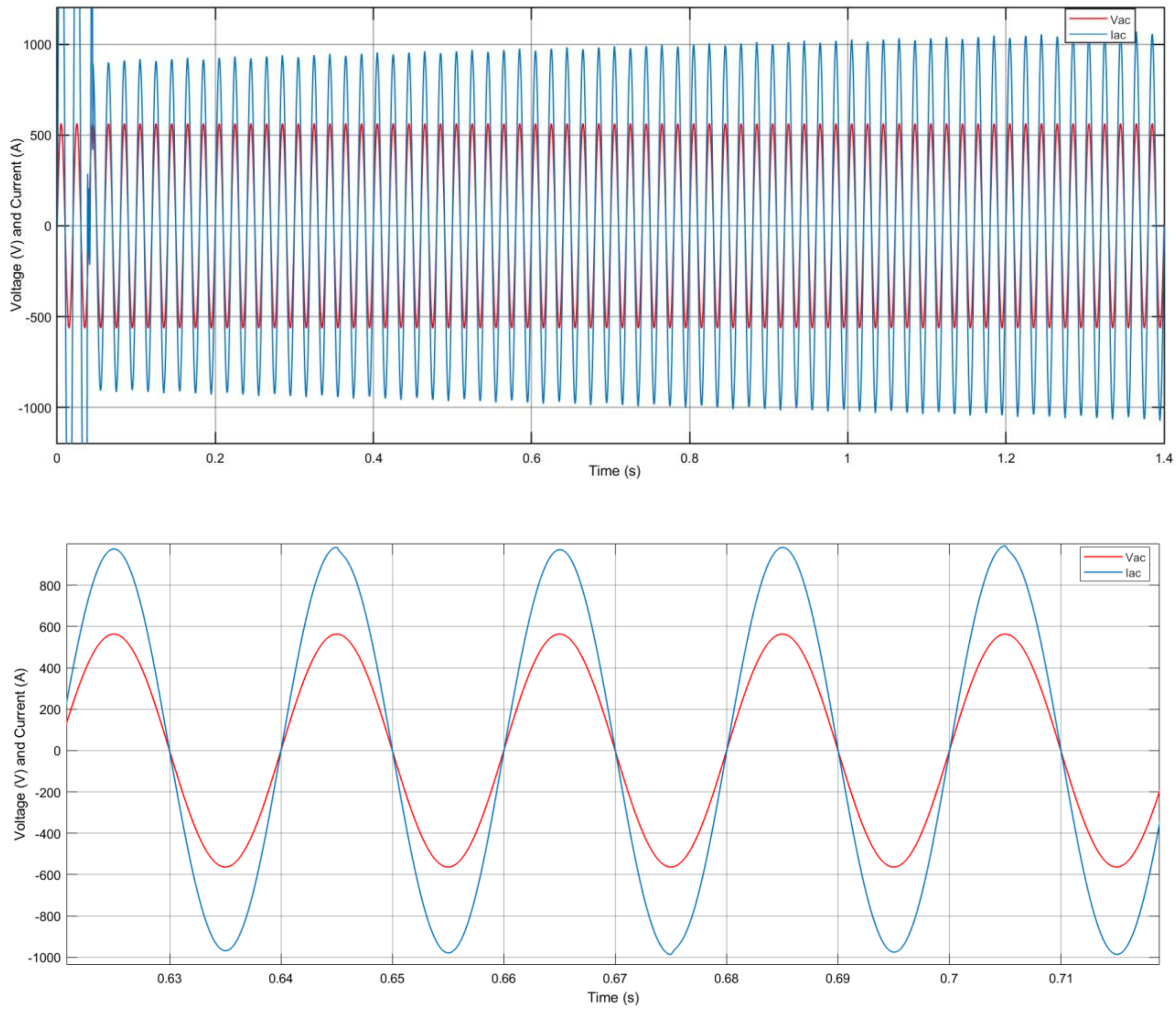

FIGURE 6: GRID CONNECTED AC VOLAGE AND CURRENT WAVEFORM

V. CONCLUSIONS

This paper has presented an advanced adaptive frequency splitting coordination control strategy for a Hybrid Energy Storage System (HESS) comprising BESS and supercapacitors to address the challenges of high-frequency PV power fluctuations in microgrids. By implementing adaptive frequency-splitting algorithm based on an Adaptive Low-Pass Filter (ALPF), the system successfully decouples energy and power requirements. The proposed strategy reduces PV ramp rates by over 75%, effectively mitigating the cloud-edge effect that typically destabilizes microgrid frequency and voltage. By diverting high-frequency transients to the supercapacitor, the battery's peak current and RMS current stress are reduced by 42.5% and 38.5%, respectively. This significantly minimizes micro cycling, which is a primary driver of electrochemical degradation. The integration of feed-forward compensation and adaptive SoC management ensures that the DC bus voltage remains within a 1.2% deviation range, even during extreme weather transitions. Unlike fixed-filter methods, the adaptive logic prevents supercapacitor saturation, ensuring the HESS remains ready to handle consecutive power bursts without depleting its energy reserves.

AI DISCLOSURE STATEMENT.

This is to acknowledge that the Author did not use any AI tool in the cause of this research.

References

[1] Papageorgiou, Asterios, Archana Ashok, Tabassom Hashemi Farzad, and Cecilia Sundberg. "Climate change impact of integrating a solar microgrid system into the Swedish electricity grid." *Applied Energy* 268 (2020): 114981.

[2] R. Khan *et al*., "Energy Sustainability–Survey on Technology and Control of Microgrid, Smart Grid and Virtual Power Plant," in *IEEE Access*, vol. 9, pp. 104663-104694, 2021, doi: 10.1109/ACCESS.2021.3099941.

[3] Bai, Fandi, and Kewei Zhang. "The research progress on distributed generation and microgrid system stability: Progress, challenges, and frontier directions," *Advances in Resources Research,* vol. 5, no. 4, pp. 2366-2408, 2025.

[4] S. Sepasi, C. Talichet and A. S. Pramanik, "Power Quality in Microgrids: A Critical Review of Fundamentals, Standards, and Case Studies," in IEEE Access, vol. 11, pp. 108493-108531, 2023, doi: 10.1109/ACCESS.2023.3321301.

[5] Lai, Chun Sing, Youwei Jia, Loi Lei Lai, Zhao Xu, Malcolm D. McCulloch, and Kit Po Wong. "A comprehensive review on large-scale photovoltaic system with applications of electrical energy storage." *Renewable and Sustainable Energy Reviews, vol.* 78, pp. 439-451, 2017.

[6] Datta, Ujjwal, Akhtar Kalam, and Juan Shi. "A review of key functionalities of battery energy storage system in renewable energy integrated power systems." *Energy Storage* vol. 3, no. 5, e224, 2021.

[7] Aghmadi, Ahmed, and Osama A. Mohammed. "Energy storage systems: technologies and high-power applications." *Batteries* vol. 10, no. 4, 141, 2024.

[8] Menye, Joselyn Stephane, Mamadou-Baïlo Camara, and Brayima Dakyo, "Lithium Battery Degradation and Failure Mechanisms: A State-of-the-Art Review" *Energies, vol.* 18, no. 2: 342, 2025, https://doi.org/10.3390/en18020342.

[9] Y. Khan, I. Idrisov, M. Pugach and F. Martin Ibanez, "Real-Time Analysis of Battery State of Health in Supercapacitor-Battery Hybrid Systems for Electric Motorcycles," in *IEEE Access*, vol. 12, pp. 151403-151414, 2024, doi: 10.1109/ACCESS.2024.3478375.

[10] J. Huang, X. Fang, X. Zhou, J. Tan, S. Dong and A. Hoke, "Battery Degradation Modeling in Hybrid Power Plants: An Island System Unit Commitment Study," *2023 IEEE Kansas Power and Energy Conference (KPEC)*, Manhattan, KS, USA, pp. 1-5, 2023, doi: 10.1109/KPEC58008.2023.10215443.

[11] Wentao Xu, Jiangong Zhu, Jie Zhang, Mengshu Tian, Jixiang Cai, Hang Wu, Gang Wei, Tingfeng Chen, Xuezhe Wei, Haifeng Dai, "Investigation of lithium-ion battery degradation by corrected differential voltage analysis based on reference electrode", Applied Energy, Vol. 389, 125735, 2025, ISSN 0306-2619, https://doi.org/10.1016/j.apenergy.2025.125735.

[12] Jadhav, V. V., Mane, R. S., & Shinde, P. V. (2020). *Bismuth-Ferrite-Based Electrochemical Supercapacitors*. Springer International Publishing. https://doi.org/10.1007/978-3-030-16718-9.

[13] H. Maghfiroh, O. Wahyunggoro and A. I. Cahyadi, "Optimal Sizing and Improved Low-Pass Filter Energy Management for Hybrid Energy Storage Electric Vehicles," in *IEEE Access*, vol. 12, pp. 180926-180938, 2024, doi: 10.1109/ACCESS.2024.3509481.

[14] M. Masih-Tehrani, M. R. Ha'iri Yazdi, V. Esfahanian, M. Dahmardeh and H. Nehzati, "Wavelet-based power management for hybrid energy storage system," in *Journal of Modern Power Systems and Clean Energy*, vol. 7, no. 4, pp. 779-790, July 2019, doi: 10.1007/s40565-019-0529-2.

[15] C. Jia, J. Cui, W. Qiao and L. Qu, "Real-Time Model Predictive Control for Battery-Supercapacitor Hybrid Energy Storage Systems Using Linear Parameter-Varying Models," in *IEEE Journal of Emerging and Selected Topics in Power Electronics*, vol. 11, no. 1, pp. 251-263, Feb. 2023, doi: 10.1109/JESTPE.2021.3130795.

[16] SadolaluBoregowda, V.K., Shree, R., Ranjana *et al.* Enhancing DC microgrid performance with fuzzy logic control for hybrid energy storage system. *SIViP* **18**, pp. 4505–4514, 2024. https://doi.org/10.1007/s11760-024-03090-8.

[17] Anudeep, K., Parimi, A.M., Deshmukh, S.S. *et al.* Designing an Intelligent Power Coordinate Controller for Hybrid Energy Storage Devices Using Machine Learning Algorithms in Electric Vehicle Application. *Arab J Sci Eng* , 2026. https://doi.org/10.1007/s13369-026-11127-y

[18] Mukalu Sandro Masaki, Lijun Zhang, Xiaohua Xia, "Fuzzy logic control of plug-in supercapacitor storage for thermoelectric management of batteries", Renewable Energy Focus, Vol. 43, pp. 59-73, 2022, ISSN 1755-0084, https://doi.org/10.1016/j.ref.2022.08.010.

[19] A. Choumal, M. Rizwan and S. Jha, "A Unified Prediction-Dispatch Framework for PV Power Scheduling Using Reinforcement Learning,"

in *IEEE Transactions on Consumer Electronics*, vol. 71, no. 4, pp. 10235-10247, Nov. 2025, doi: 10.1109/TCE.2025.3619248.

[20] F. Härtel and T. Bocklisch, "Minimizing Energy Cost in PV Battery Storage Systems Using Reinforcement Learning," in *IEEE Access*, vol. 11, pp. 39855-39865, 2023, doi: 10.1109/ACCESS.2023.3267978

[21] Souad Lidaighbi, Mustapha Elyaqouti, Dris Ben Hmamou, Driss Saadaoui, Khalid Assalaou, Elhanafi Arjdal,"A new hybrid method to estimate the single-diode model parameters of solar photovoltaic panel", Energy Conversion and Management: X, vol 15, 100234, 2022, ISSN 2590-1745, https://doi.org/10.1016/j.ecmx.2022.100234.

[22] Raszmann, Emma, Kyri Baker, Ying Shi, and Dane Christensen. "Modeling stationary lithium-ion batteries for optimization and predictive control." In *2017 IEEE power and energy conference at illinois (PECI)*, pp. 1-7. IEEE, 2017.

[23] M. Tariq, A. I. Maswood, C. J. Gajanayake and A. K. Gupta, "Modeling of a Li-ion battery energy storage system using an optimal harmonic number based model of DC-DC converter for more electric aircraft," *IECON 2016 - 42nd Annual Conference of the IEEE Industrial Electronics Society*, Florence, Italy, 2016, pp. 4429-4434, doi: 10.1109/IECON.2016.7793657.

[24] María F. Quintana, Enrique E. Valdés Zaldívar, Joaquín F. Pedrayes, V. Fajardo Latorre, Manés F. Cabanas, Gonzalo A. Orcajo, "Equivalent circuit modeling of a supercapacitor bank with variable capacitance and lossless dynamic balancing", Results in Engineering, vol. 27, 106966, 2025, ISSN 2590-1230, https://doi.org/10.1016/j.rineng.2025.106966.

[25] J. G. Parada Salado, C. A. Herrera Ramírez, A. G. Soriano Sánchez, and M. A. Rodríguez Licea, "Nonlinear Stabilization Controller for the Boost Converter with a Constant Power Load in Both Continuous and Discontinuous Conduction Modes," *Micromachines*, vol. 12, no. 5, p. 522, May 2021. Doi: 10.3390/mi12050522.

[26] P. N. Robin and S. Barua, "A Decentralized Energy Solution: PV-Battery-Supercapacitor Hybrid Approach for Rural Communities," *2024 27th International Conference on Computer and Information Technology (ICCIT)*, Cox's Bazar, Bangladesh, 2024, pp. 826-830, doi: 10.1109/ICCIT64611.2024.11021909

[27] National Renewable Energy Laboratory. (2025). *System Advisor Model (SAM)* (Version 2025.4.16) [Software]. Available from https://sam.nrel.gov/

[28] Nigerian Meteorological Agency (NiMet). (2024). *Daily Solar Radiation Records for Kano and Lagos Stations (2010–2023)*. [Dataset]. Abuja, Nigeria.